



Study on the Effect of Dry–Wet Cycles on Dynamic Mechanical Properties of Sandstone Under Sulfuric Acid Solution

Xin Huang¹ · Jianyong Pang² · Jiuqun Zou²

Received: 26 July 2021 / Accepted: 15 November 2021 / Published online: 17 January 2022
© The Author(s), under exclusive licence to Springer-Verlag GmbH Austria, part of Springer Nature 2021

Abstract

The influence of water–rock interaction in the process of coal mine construction cannot be ignored, especially when the groundwater quality is complex and contains acidic substances. In this paper, considering the influence of mining, blasting, and earthquake, the dynamic mechanical properties and fractal characteristics of sandstone under acid dry–wet cycle were studied. A comprehensive method combining X-ray diffraction (XRD), scanning electron microscopy (SEM), and energy dispersive spectrometer mapping (EDS Mapping) technology for chemical damage analysis was established, and the damage mechanism of sandstone was summarized. The test results show that the acid dry–wet cycle has a great influence on the dynamic peak stress of sandstone (σ_d) and elastic modulus (E_d) is higher than neutral. And with the decrease of pH value of acidic solution, σ_d and E_d decrease and the peak strain increases, indicating that the acid solution has corrosion and softening effect on sandstone. With the increase of acid dry–wet cycles, the fractal dimension increases linearly. Sandstone fragments show more broken blocks and smaller particle sizes. Microscopic comprehensive analysis shows that acid solution (H_2SO_4) will preferentially react with metal oxides and salt cements to open rock pores, and gypsum ($CaSO_4$) and other products will be formed in the process. In the process of the acid dry–wet cycle, the sandstone is corroded by acid solution, which leads to pore growth. Meanwhile, the dry–wet cycle causes repeated expansion and contraction of rock particles. Both of them accelerate rock failure.

Highlights

- (1) Acid solution weakens the dynamic mechanical parameters of rock, softens the specimen and increases the post-peak strain.
- (2) With the increase of cycles, the fractal dimension of sandstone increases linearly, and the lower the pH, the more fragmentation and the smaller the particle size.
- (3) The damage caused by the acid dry–wet cycle to the rock consists of two parts: physical and chemical.

Keywords Acid dry–wet cycle · Dynamic mechanical parameters · Fractal dimension · EDS mapping · Chemical damage mechanism

✉ Xin Huang
xinh@cumt.edu.cn

✉ Jianyong Pang
jypang@aust.edu.cn

¹ State Key Laboratory for Geomechanics and Deep Underground Engineering, China University of Mining and Technology, Xuzhou 221116, China

² School of Civil Engineering and Architecture, Anhui University of Science and Technology, Huainan 232001, China

1 Introduction

Water is an important link between the lithosphere, biosphere, and atmosphere. Water–rock interaction is one of the important driving forces for the evolution of the near-surface environment. Under the coupling effect of chemistry and mechanics, it greatly affects the stability of stratum structure and the evolution of the groundwater environment (Ciantia et al. 2015; Critelli et al. 2014). With the development of infrastructure construction, many geotechnical engineering,

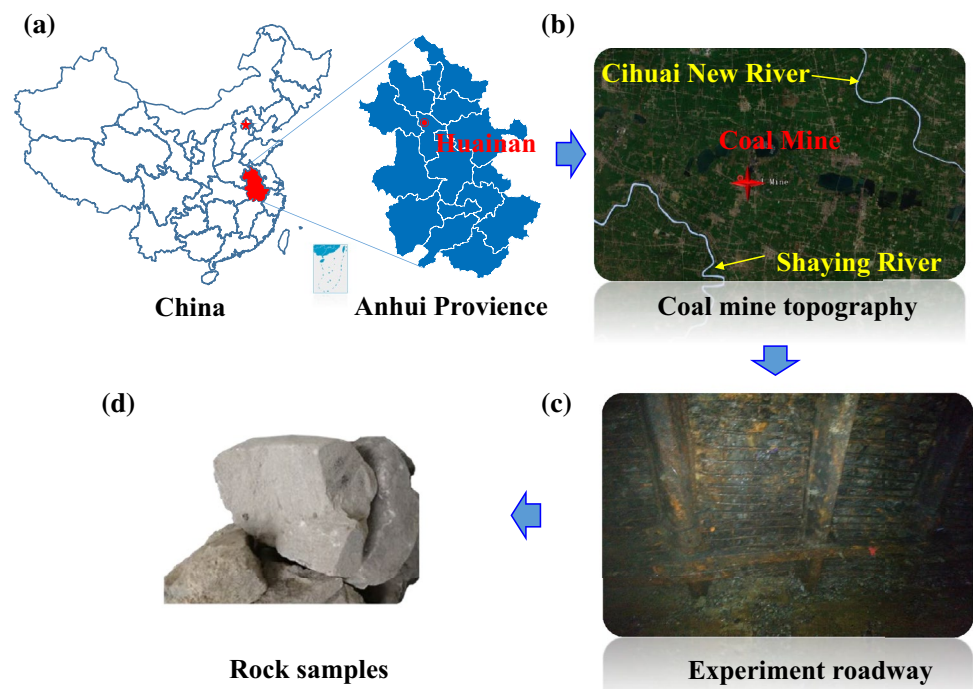
such as tunnel construction, bridge engineering, water conservancy engineering, and deep mining engineering, are faced with the influence of dry–wet cycle caused by complex hydrological conditions, such as groundwater level rise and fall (Liu et al. 2018a), rainfall evaporation (Liu et al. 2020), and water level fluctuation in reservoir area (Fang et al. 2019; Jiang et al. 2019; Liu et al. 2016).

However, the water in nature is not all neutral. For example, in Southwest China, acid rain is dominant all the year-round, which causes great damage to historical sites (Longmen Grottoes, the world cultural heritage (Wang et al. 2017)). Moreover, acid rain often causes long-term corrosion to cave rocks after it seeps into the ground, which is still unsolvable. In recent years, many scholars have begun to carry out a lot of research on this aspect (Fang et al. 2019; He et al. 2020; Hu et al. 2019; Meng et al. 2019) and found that the acidic environment is more likely to lead to rock damage. Liu et al. (2019) showed that the coupling effect of acid rain and dry–wet cycle on the disintegration speed of granite residual soil is much higher than that of a single factor. Han et al. (2019a) found that the damaging effect of the dry–wet cycle under acid corrosion on the uniaxial compressive strength of red sandstone is higher than that under a neutral environment. The tests of Liang and Fu (2020) also showed that the decrease range of tensile fracture strength of sandstone in an acid environment is greater than that in alkaline and neutral environment. For this research, Dehestani et al. (2020) analyzed the mechanism of sandstone tensile (type I) and sliding (type II) fractures under acid dry–wet cycles from the perspective of mineralogy and porosity. Liang et al. (2021) further studied the fracture characteristics of rocks under alkaline dry–wet cycles, and its impact on the degradation of sandstone fracture toughness is between acidic and neutral. Han et al. (2019b) considered that the damage of chemical solution to rock is reflected in the development of cracks, and the inclination angle of cracks is the main factor of crack development. The sulfuric acid solution can accelerate the development of cracks and cause damage. Yuan et al. (2019a) deduced the chemical equation of sandstone reaction in acid solution from the micro-level according to the change of ion concentration before and after the reaction and the formation rate, and explained the reason for the decrease of its shear strength. Sun and Zhang (2019) proposed color brightness and thermal conductivity to evaluate the influence of the dry–wet cycle on sandstone stability under chemical solution. Both of them decreased with the increase in the number of cycles. In addition to surface acid deposition, deep groundwater is also easy to be converted into an acidic solution after dissolving minerals. In previous research, the author has carried out experimental research on uniaxial mechanical parameter change and damage mechanism of deep roadway surrounding rock (Huang et al. 2020). Guo et al. (2020) studied the failure law of roadway surrounding rock under dry–wet cycle

through a similar simulation test, and found that the failure process expanded from the roof to the two sides. However, in a summary of the above studies, the static mechanical properties of rock samples in a chemical environment are mostly studied, but the research on the acid dry–wet cycle of rock under a high strain rate is far from enough. Cai et al. (2021) found that the presence of water can effectively absorb the energy of rock bursts and prevent rock bursts from occurring to a certain extent. Zhou et al. (2017) first establish the decay model of rock strength and accurately predict the rock strength considering rate dependence and cyclic degradation. Du and Bai (2019), Du et al. (2019) studied the degradation law of dynamic tensile strength of red sandstone after dry–wet cycle, and predicted its long-term strength value based on the test results. Li et al. (2019) used DIC (digital image correlation) technology and a high-speed camera to analyze the tensile failure morphology of rock samples after drying and wetting cycles, revealing the reason for the decrease of dynamic tensile strength of sandstone. Yuan et al. (2019b) also draw corresponding conclusions, and according to SEM images, cyclic loading and unloading of tensile stress in the process of water adsorption and desorption are the main reasons for the generation and propagation of microcracks. The research of Zhou and Cai et al., showed that the dry–wet cycle has a weakening effect on the physical properties, tensile strength (Zhou et al. 2018) and fracture strength (Cai et al. 2020a) of sandstone. The above study is limited to the influence of the dry–wet cycle, and the acid environment is not considered. In addition, the research object is only a few rock samples, and the dynamic mechanical properties of different rock types need to be enriched (Cai et al. 2020b; Zhou et al. 2020). Therefore, this paper selects sandstone as the research object to study the influence of acid environment and dry–wet cycle coupling on samples under high strain rate, to provide a reference for related research.

In addition to the research object and method, the damage mechanism of the acid dry–wet cycle on rock samples is also the focus of many scholars. Ma et al. (2020) combined CT technology with ultrasonic inspection technology and proposed a non-destructive and visual method to study the damage process of slate under dry–wet cycle. Chen et al. (2018) proposed to use DIC technology to measure non-contact deformation, and it was also applied in reference (Li et al. 2019). Liu et al. (2018b) used PFC 2D discrete element software to conduct a combined study of micro-test and microscopic simulation. The above researches were based on the macroscopic or microscopic research on the damage mechanism, and the content is mostly the change of physical morphology. In this paper, based on microscopy technology, XRD and SEM were used to determine the material composition and micro-morphology, and then combined with EDS Mapping technology to scan the damage interface, drew the

Fig. 1 Sample position: **a** site of rock in Huainan, Anhui Province, China, **b** coal mine location, **c** water environment in coal mine roadway, and **d** the rock samples



element phase distribution map, and proposed a comprehensive analysis of chemical damage method.

In this paper, the surrounding rock (sandstone) of the coal mine roadway is taken as the research object, which is treated by dry–wet cycle in sulfuric acid solution with $\text{pH} = 3, 5, 7$. The one-dimensional impact test of sandstone after different cycles is carried out. In addition, XRD, SEM, and EDS Mapping analyses were carried out on sandstone before and after the reaction. The dynamic strength and fracture morphology of sandstone under an acid environment were analyzed from the macroscopic and the chemical damage process and mechanism were discussed from the microscopic.

2 Materials and Methods

2.1 Preparation of Sandstone Specimen

As a kind of underground engineering greatly affected by geology, the safety and stability of coal mines have always been the focus of scientific workers. In this paper, the samples were taken from a coal mine in Huainan City, Anhui Province, China (see Fig. 1a). The coal mine is located in the alluvial plain of Huaihe River, with flat terrain, and the ground elevation is generally about +24 to +26 m (see Fig. 1b). The bedrock of the minefield is covered by the quaternary loose layer. Due to the uneven development of fissures and weak

water yield, the water seepage in the inner wall of the roadway will occur in the quaternary middle Pleistocene pore water-bearing group, Permian sandstone fissure water-bearing group, and carboniferous Taiyuan limestone karst fissure water-bearing group, which has a great impact on the stability of the roadway. The roadway had been affected by groundwater infiltration for a long time, the surrounding rock of the surrounding rock had expanded, and the supporting structure had been deformed (see Fig. 1c). The apparent characteristics of the rock sample are gray-white, few nodules, and a few dark brown spots (see Fig. 1d).

The XRD and thin section identification tests were carried out to understand the mineral composition, grain size, and structure of the samples. The Smartlab High-Resolution X-ray diffractometer was used to analyze the diffraction patterns of sandstone, the main components are quartz, feldspar, kaolinite, and limestone (see Fig. 2a). Thin sections of rock with length \times width \times thickness = 30 mm \times 20 mm \times 0.03 mm were prepared. The thin sections were observed under an Ortho Polarizing Microscope. The identification results showed that the rock sample is of fine-grained sand structure with pore cementation. The quartz content of the rock sample is 70%, the clay mineral is 15%, the siliceous rock is 10%, and the feldspar is 5%. The scattering distribution of quartz can be observed on the thin section. The filler is argillaceous impurity with a small amount of calcareous cement (see Fig. 2b).

According to the suggestion of ISRM (the International Society of Rock Mechanics and Rock Engineering) (ISRM

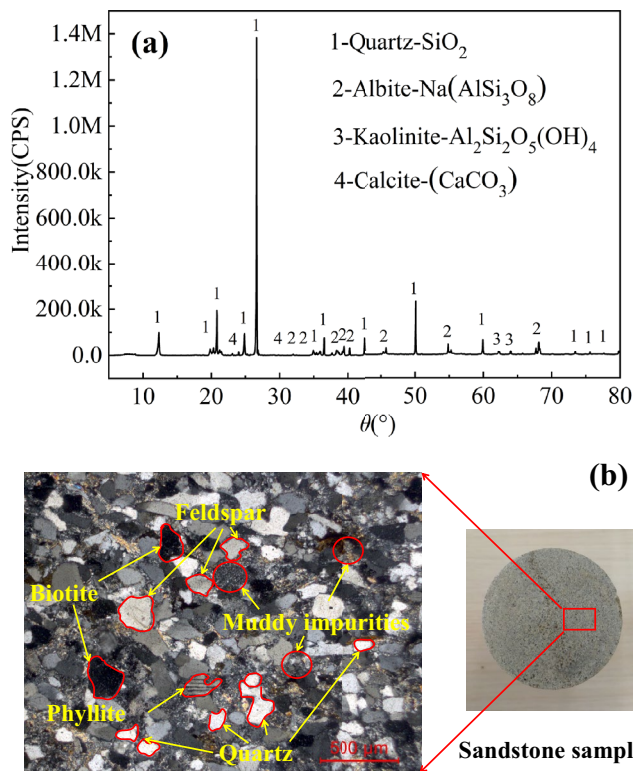


Fig. 2 Sample composition detection: **a** XRD analysis of sandstone composition, and **b** results of thin section identification

1981), the specimens were processed into a cylinder with a diameter of 50 mm and a height of 25 mm for a one-dimensional impact test. After grinding, the surface flatness of the specimen was controlled within ± 0.05 mm, and the vertical deviation of the upper and lower surfaces was controlled within $\pm 0.25^{\circ}$ (see Fig. 3).

The wave velocities of the specimens selected to participate in the experiment were between 4.55 and 4.70 km/s to ensure that their densities are similar, and these specimens were divided into 4 groups, of which 3 groups were the test group and 1 group was the control group. The basic physical parameters of the specimens are shown in Table 1.

2.2 Experimental Method and Procedure

1. Preparation for an acidic solution

12 L solutions with pH = 3, 5 were prepared with H₂SO₄ solution for soaking sandstone, respectively. The

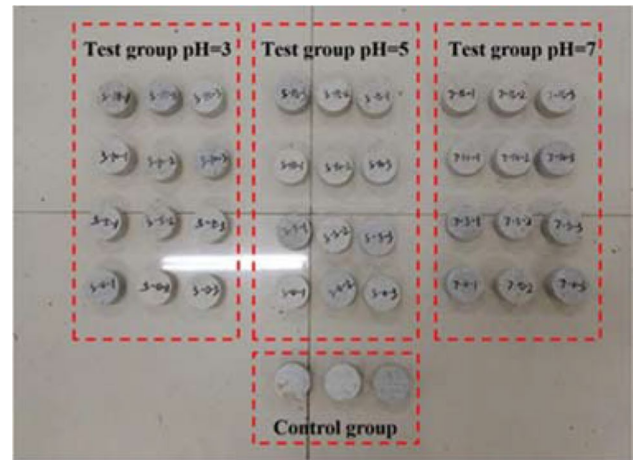


Fig. 3 Experimental specimens

solution with pH = 7 was the tap water provided by an ordinary urban water supply network.

2. Design of dry-wet cycle

Test group: The specimens were divided into 3 groups, which were immersed in the solution with pH of 3, 5, and 7, and each group was further divided into 4 groups, which were treated in four stages: stage I (5 d solution immersion), stage II (0–5 cycles), stage III (5–10 cycles), and stage IV (10–15 cycles), 3 specimens as a group, a total of 36 specimens.

Control group: Without any treatment, it was made of natural sandstone after cutting and grinding, a total of 1 group, 3 specimens.

According to the grouping scheme, the treatment process was as follows: soak each group of specimens in the solution with different pH values for 12 h, and then put them into the hot air circulation drying oven to dry for 12 h, which is regarded as one cycle of dry-wet. The temperature of the drying oven was set at 105 °C to ensure that the water in the specimen can be completely evaporated (see Fig. 4).

2.3 SHPB Devise and Basic Principle

The Split Hopkinson Pressure Bar (SHPB) used in this experiment is mainly composed of 3 main systems: driving system, bar system, and data acquisition system. During the impact test, the impact bar is driven by the pressure

Table 1 Basic physical properties of sandstone specimens

Basic properties	Average mass /g	Natural density g/cm ³	Dry density g/cm ³	Saturated density g/cm ³	Dry P-wave velocity km/s	Saturated P-wave velocity km/s
Value	126.55	2.496	2.477	2.642	4.523	4.774

Fig. 4 Schematic diagram of acidic wet-dry cycle process

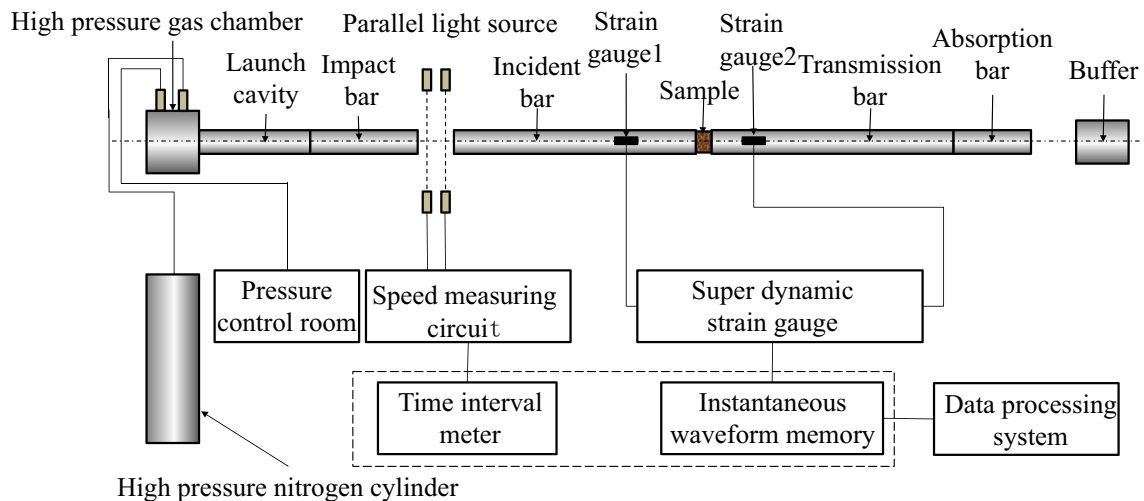
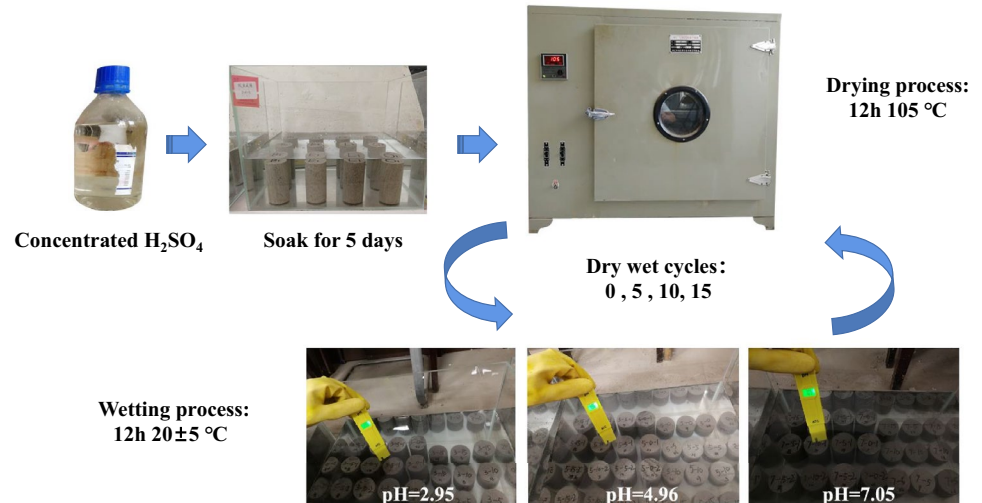


Fig. 5 Structural schematic diagram of SHPB device

produced by the instantaneous release of compressed nitrogen to impact the incident bar, forming shock waves through the sandstone specimen and entering into the transmission bar. Finally, the buffer is used to absorb the surplus energy.

The impact bar is 37 mm in diameter and 0.6 m in length, the incident bar is 50 mm in diameter and 2.4 m in length, and the transmission bar is 50 mm in diameter and 1.2 m in length. The density of each bar is 7.8 g/cm^3 , the elastic modulus is 210 GPa, the wave velocity is 5190 m/s, and Poisson's ratio is 0.30. BX120-2AA strain gauge is used to collect voltage signal, and DPO3024 digital oscilloscope and KD6009 strain amplifier are used to collect data signal. The SHPB device schematic diagram is shown in Fig. 5.

The physical diagram of the test device is shown in Fig. 6.

To eliminate the friction resistance of the end face, the two ends of the sandstone specimen were ground flat, and a layer of Vaseline lubricant was evenly applied on both sides to reduce the influence of the end face of the bar on the surface stress distribution of the specimen, to prevent the collected waveform from being disturbed and affecting the test results. The central axis of the specimen must coincide with that of the bar when installing the specimen. The gas storage control switch is pressed, when the air pressure reaches 0.4 MPa, the switch is opened to release nitrogen, and the impact test is completed. Then, after adjusting the position of the transmission bar, the incident bar, and the impact bar, the specimen is loaded again, and the next test is carried out.

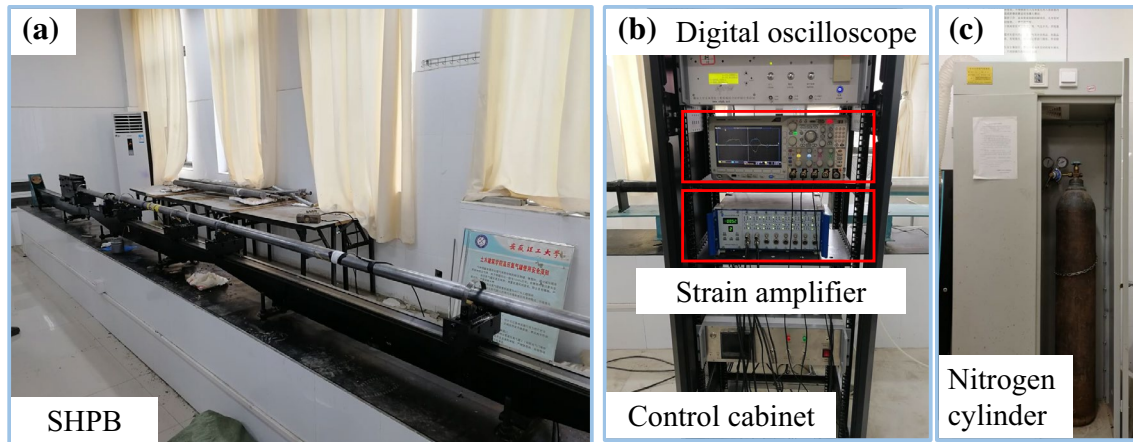


Fig. 6 Physical diagram of test equipment

3 Test Results

For rock materials, according to the research on the data processing method of low wave impedance materials (Liu et al. 1998). The original waveform signal collected was processed by the simplified three-wave method (Song and Hu 2005; Yuan et al. 2014; Zhang et al. 2020). The stress $\sigma(t)$, strain $\varepsilon(t)$, and strain rate $\dot{\varepsilon}(t)$ of sandstone specimens can be obtained as shown in Eq. (1).

$$\sigma(t) = \frac{E_0 A_0}{A_s} \varepsilon_i(t),$$

$$\varepsilon(t) = \frac{C_0}{l_s} \int_0^t [\varepsilon_i(t) - \varepsilon_r(t) - \varepsilon_t(t)] dt, \quad (1)$$

$$\dot{\varepsilon}(t) = \frac{C_0}{l_s} [\varepsilon_i(t) - \varepsilon_r(t) - \varepsilon_t(t)],$$

where $\varepsilon_i(t)$, $\varepsilon_r(t)$, and $\varepsilon_t(t)$ are the incident, reflected, and transmitted stress waves at time t , respectively. E_0 , A_0 , and C_0 are the elastic modulus, cross-sectional area, P-wave velocity of bar, respectively. A_s is the cross-sectional area of the specimen. l_s is the height of the specimen and t is the duration of the stress wave.

3.1 Analysis of Dynamic Pressure Resistance Characteristics of Sandstone

3.1.1 Dynamic Stress–Strain Curve Analysis

The dynamic stress–strain curves obtained from SHPB tests for typical sandstones in their natural state and after dry–wet cycles (n) at different pH solutions at a driving air pressure of 0.4 MPa are shown in Fig. 7. It can be observed from the

stress–strain curve diagram that after experiencing dry–wet cycles, the peak stress and elastic modulus of the sandstone are depreciated to some extent, especially in the sulfuric acid solution, where the strength depreciation is particularly severe, and the pressure–dense part of the rising section of the stress–strain curve gradually increases, while the strain after the peak point increases and the ductility is prominent.

The analysis shows that the dynamic mechanical properties of sandstone specimens subjected to acid dry–wet cycles of different pH values have deteriorated to different degrees. Comparing the same n , the acid dry–wet cycles at pH=3 showed the greatest loss of strength, followed by the test group at pH=5, with the neutral solution showing the least loss. It can be observed that the pH of the solution is an important factor in the dynamic mechanical properties of sandstone.

Based on the dynamic stress–strain curves of sandstone in solutions of different pH values, the peak strain variation curves of each group of specimens were calculated as shown in Fig. 8, and the average values were used to depict the variation trend for the sake of observation. Overall, it can be observed that in the sulfuric acid solution, as the pH decreases, the peak strain of the specimen gradually increases, with increases of 10.59% (pH=5) and 17.79% (pH=3), indicating that the acid solution has a corrosive and softening effect on the specimen, leading to an increase in internal porosity, a softening of strain, and a gradual increase in peak strain. It is also observed that the peak strain of the sandstone in neutral solution does not increase, but rather decreases, with a growth rate of -6.78% (pH=7). The reason for this phenomenon is that the softening of the specimen caused by the dry–wet cycles alone is not significant, but rather the decrease in strain values due to the decrease in peak strength, which causes brittle damage at a small impact pressure.

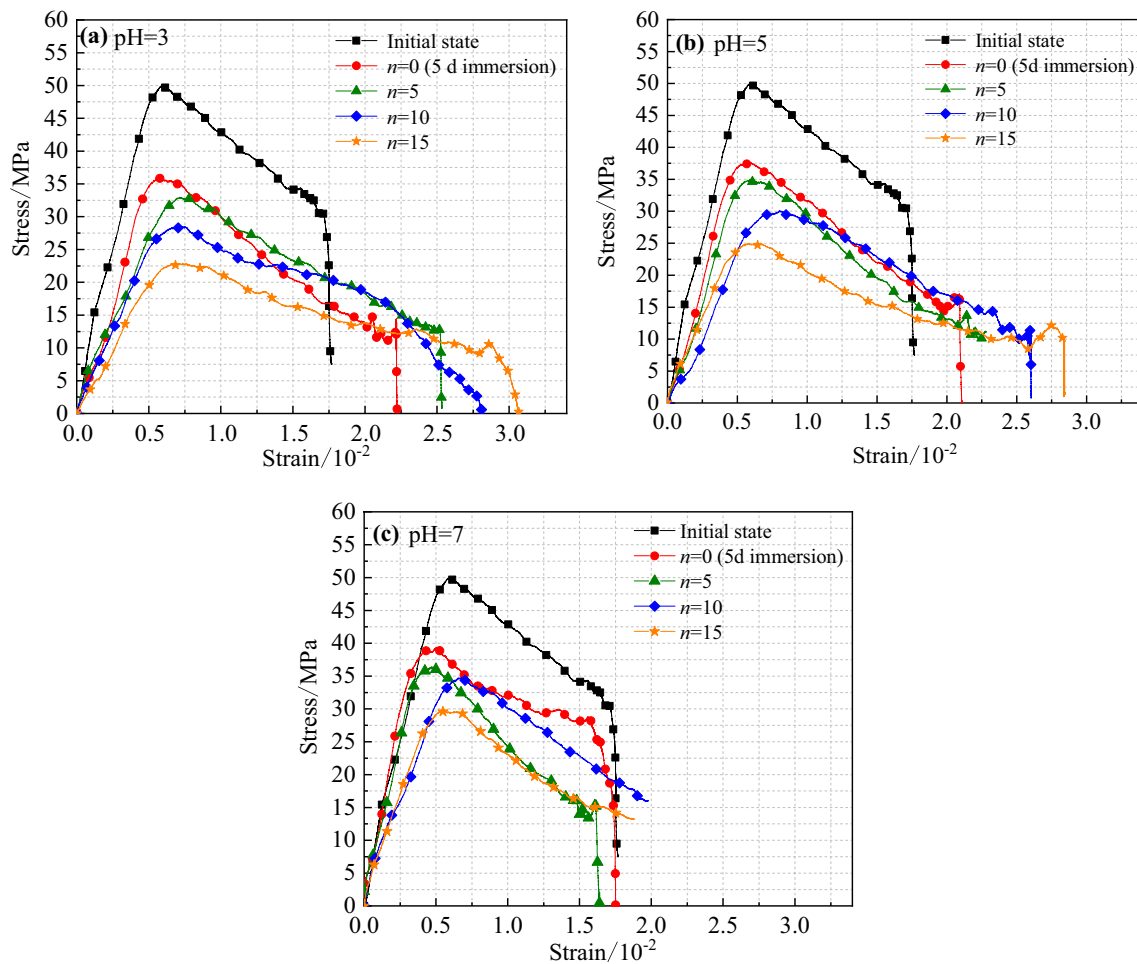


Fig. 7 Dynamic stress–strain curve of sandstone under different environments

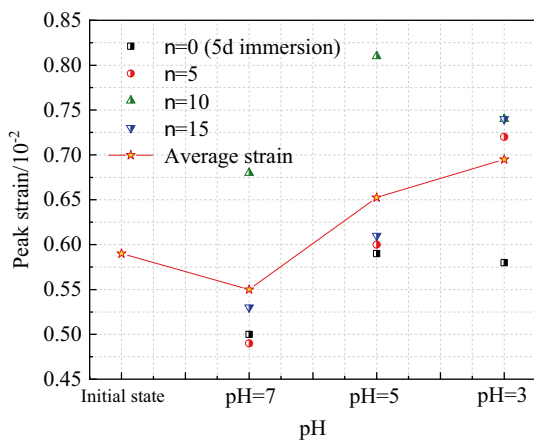


Fig. 8 Peak strain curve of specimen at different pH values

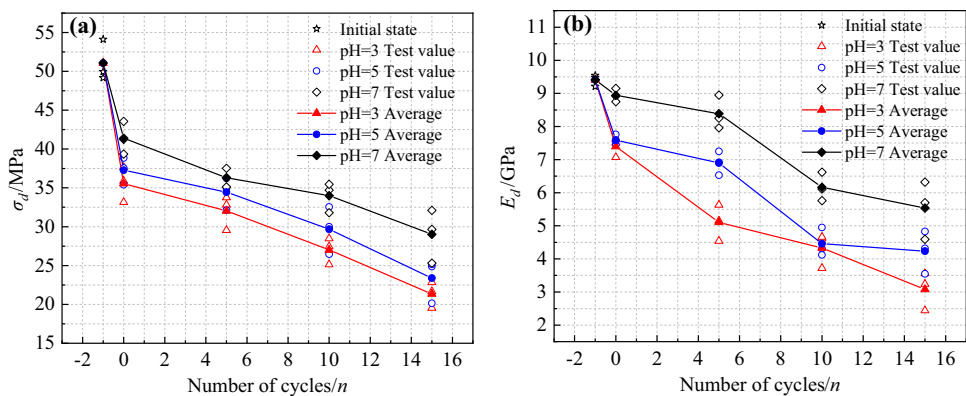
3.1.2 Deterioration Analysis of Dynamic Mechanical Parameters of Sandstone

Figure 9 shows the variation of dynamic compressive strength σ_d and modulus of elasticity E_d with the number of dry–wet cycles n for sandstone with different pH solutions.

As shown in Fig. 9, the dynamic compressive strength and modulus of elasticity of the sandstone show a tendency to decrease as n increases. A large drop in compressive strength can be observed at the beginning of the dry–wet cycle ($n=0$) (see Fig. 9a), with σ_d dropping by 18.95% (pH=7), 27.02% (pH=5), and 30.37% (pH=3), respectively. The decrease increases gradually with decreasing pH, indicating that the greater the concentration of the acidic solution, the greater the damage to the sandstone. For E_d (see Fig. 9b) the loss during the initial immersion is less for the neutral solution at 4.99% (pH=7) compared to the reduction of 19.34% (pH=5) and 21.36% (pH=3) for the acidic solution, and it can be observed that the dispersion of the data increases with increasing n , but the overall trend remains one of reduction.

According to the definition of reduction degree of mechanical parameters of specimen in reference (Deng et al. 2015), the degradation degree of dynamic mechanical

Fig. 9 Dynamic compressive strength and modulus of elasticity curves with number of dry–wet cycles



parameters of sandstone under acid dry–wet cycle condition is defined as P_i :

$$P_i = (T_0 - T_i) / T_0 \times 100\%, \tag{2}$$

where T_0 is the value of sandstone mechanical parameters in the initial state, including peak stress, MPa, and elastic modulus, GPa; T_i is the mechanical parameter value after the i th dry–wet cycle.

As shown in Fig. 10a, b, the deterioration trend of dynamic compressive strength and modulus of elasticity of sandstone, respectively. Overall, the degree of deterioration of each group of specimens is gradually increasing as n increases, and the increasing trend is linear, compared to the higher degree of deterioration of E_d . In addition, the deterioration of the dynamic mechanical parameters of the sandstone in the acidic solution is higher than that of the sandstone in the neutral solution at all stages of the cycle, with a progressive increase in deterioration as the pH decreases. The fitting of the deterioration curves for each group of specimens shows that the slope of the fitted curve is increasing as the pH decreases, for example, the rate of increase of the deterioration curve for σ_d shows 1.87 (pH=3) > 1.82 (pH=5) > 1.54 (pH=7) and similarly for E_d , 2.92 (pH=3) > 2.66 (pH=5) > 2.64 (pH=7). This suggests

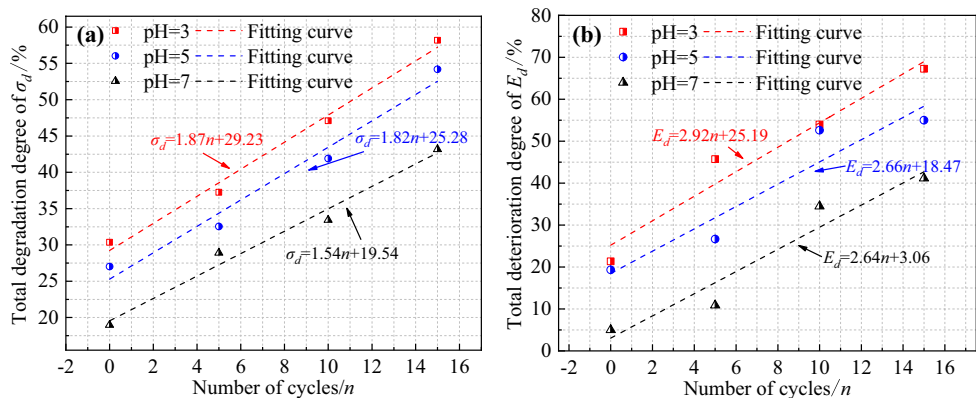
that the damage caused to the specimens is accelerated and cumulative as the acidic strength increases, with the sulfuric acid solution significantly accelerating the damage to the sandstone.

3.2 Analysis of Sandstone Fragmentation

The sandstone specimens were damaged and fractured after impact. The damaged specimens were collected to compare the degree of fragmentation. The images of sandstone after the dry–wet cycle in acid solution with different pH values are shown in Fig. 11.

The size and shape of sandstone fragments under different acid dry–wet cycle conditions are different. When the pH value of the solution is the same, with the increase of cycles, the number of fragments increases and the volume of fragments decreases. When the number of dry–wet cycles is the same, with the decrease of pH value, the fragmentation of sandstone specimen becomes more and more serious, and the fragment particles become fine. Both acid solution and dry–wet cycle lead to the decrease of the degree of bond and dynamic compressive strength of sandstone. To analyze the degree of fragmentation, the fragments of the broken specimens were collected and analyzed by fractal characteristics.

Fig. 10 Degradation curve of mechanical parameters of sandstone under impact load



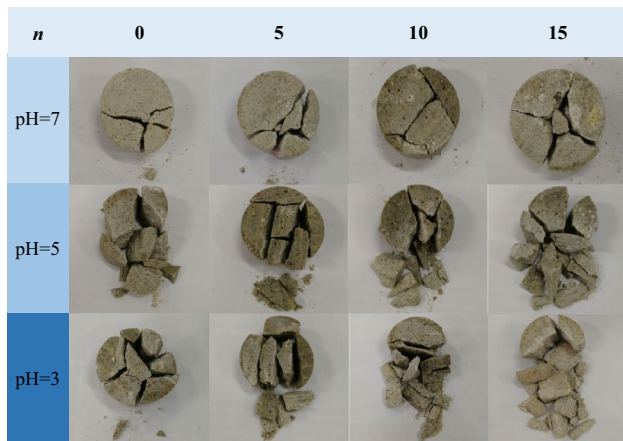


Fig. 11 Fracture of sandstone after impact test

3.3 Fractal Characteristics of Sandstone Fragments

The fragments of each specimen were successively passed through 14 grades of standard sieves with pore sizes of 40.0 mm, 31.5 mm, 26.5 mm, 19.0 mm, 10.0 mm, 5.0 mm, 4.75 mm, 2.5 mm, 2.36 mm, 1.25 mm, 0.63 mm, 0.315 mm,

0.3 mm, and 0.16 mm. The fragments of each stage of the standard sieve were put on the electronic balance to weigh the weight (accuracy 0.001 g), and the percentage (c) of the total mass of the specimen. The fragmentation distribution of sandstone with different cycle times and acid solution concentrations are shown in Fig. 12.

Under different pH conditions, the slope of the specimen distribution curve increases with the increase of dry–wet cycles, which indicates that the number of small- and medium-sized fragments increased, while the number of large-sized fragments decreases. Comparing with the initial sandstone distribution curve, with the decrease of pH value, the rate of curve slope growth gradually increases. When pH = 3, fragmentation is the most serious. The particle size of the fragments mainly concentrates in the range of 0–31.5 mm after 15 cycles.

To more clearly describe the distribution of sandstone fragmentation after receiving impact load, the average fragment size degree d_m is used to describe the fragmentation degree of sandstone under the action of the acid dry–wet cycle (Xu and Liu 2012):

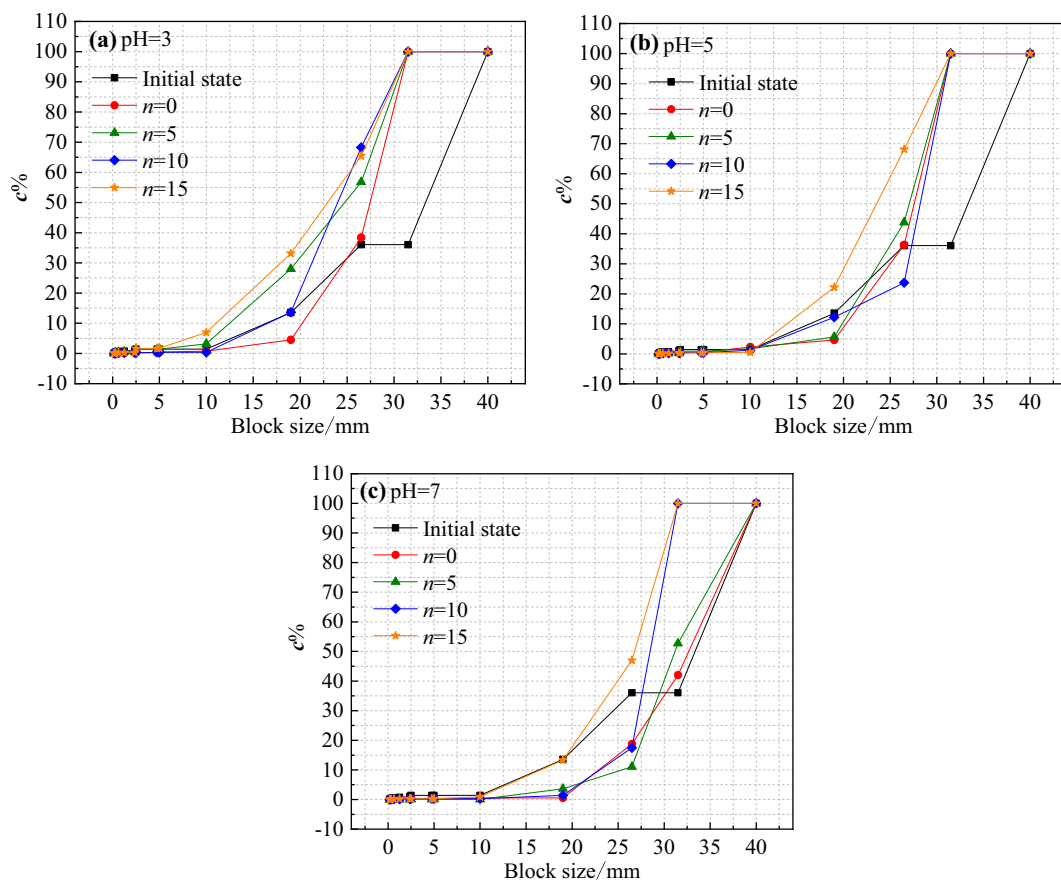


Fig. 12 Distribution curve of dry–wet cycles and sandstone fragmentation under different pH values

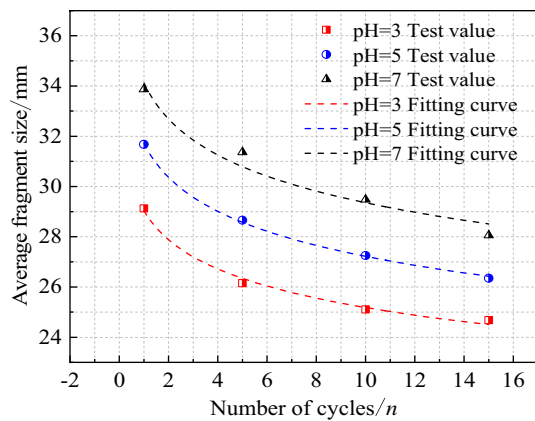


Fig. 13 Average fragment size distribution of sandstone

Table 2 Fitting results of average fragment size curve of sandstone

pH	Fitting curve	R^2
3	$d_m = 27.57 + 1.47(1 - 1.34\ln(n))$	0.99
5	$d_m = 15.93 + 15.79(1 - 0.12\ln(n))$	0.99
7	$d_m = 17.13 + 16.99(1 - 0.12\ln(n))$	0.97

$$d_m = \frac{\sum (r_i d_i)}{\sum r_i}, \quad (3)$$

where d_i is the average size of rock fragments in the standard sieve with different particle sizes; r_i is the mass percentage of rock fragments corresponding to d_i .

The average fragment size curves of sandstone specimens under different acid dry–wet cycles are shown in Fig. 13.

According to Eq. (3), the average fragment size under the initial state is 35.37 mm, which is larger than that of sandstone specimens after acid dry–wet cycle treatment. As shown in Fig. 13, with the increase of acid solution concentration, the average fragment size of sandstone specimens decreases in turn. Meanwhile, the average fragment size of sandstone under different acid concentrations decreases with the increase of dry–wet cycles, and the decreasing rate decreases with the increase of cycles and tends to be gentle gradually. Assuming that the transformation of the average fragment size of the specimen with the number cycles n is continuous, the logarithmic function $y = a + b(1 - \ln(n))$ is used to fit the changes of average fragment size of sandstone under different pH values. The results are shown in Table 2.

3.4 Fractal Dimension Analysis of Fragments

Fractal geometry was proposed by the French mathematician B.B.Mandelbrot in the 1970s. It is mainly used to study irregular shape materials. Recently, the fractal theory has

been widely used in rock mechanics because of its good fractal structure (Li et al. 2018).

According to the Mass–Frequency relationship (Shan and Li 2003), the distribution equation of rock fragmentation can be obtained, as shown in Eq. (4):

$$Y = \frac{M(x)}{M_T} = \left(\frac{x}{x_m} \right)^{3-D_b}, \quad (4)$$

where x is the grain size of sandstone particles; x_m is the maximum size of fragments; D_b is the fractal dimension of fragmentation distribution; $M(x)$ is the cumulative mass of fragments smaller than x ; M_T is the total mass of fragments.

By taking logarithms on both sides of Eqs. (4), (5) can be obtained:

$$\lg Y = \lg \left[\frac{M(x)}{M_T} \right] = (3 - D_b) \lg \left(\frac{x}{x_m} \right). \quad (5)$$

According to Eq. (5), the $\lg[M(x)/M_T] - \lg x$ curve is linearly fitted, and its slope is $(3 - D_b)$, where D_b is the fractal dimension of impact fracture of specimens with different dry–wet cycles in different pH acid solutions.

As shown in Fig. 14, the fractal dimension of sandstone specimens ranges from 0.866 to 1.910. Among them, the minimum fractal dimension of sandstone in the initial state is 0.886. When pH=3, the fractal dimension of the specimen ranges from 1.484 to 1.910, with an average of 1.680; when pH=5, the fractal dimension of the specimen is between 1.473 and 1.782, with an average of 1.624; when pH=7, the fractal dimension of the specimen is between 1.411 and 1.726, with an average of 1.572. The results show that the fractal dimension of sandstone decreases with the increase of pH. The large fractal dimension indicates that the sandstone has a high degree of fragmentation, a large number of fragments, a small size, and a high degree of damage.

When pH=3, 5, and 7, the relationship between the number of cycles and fractal dimension is shown in Fig. 15.

It can be observed that the fractal dimension increases with the increase of dry–wet cycles, and presents a linear trend. The fractal dimension of each cycle showed the characteristics of pH=3 > pH=5 > pH=7. These characteristics are also consistent with the distribution of macro fracture morphology. The larger the fractal dimension, the higher the degree of fragmentation.

4 Discussion on the Mechanism of Chemical Damage During Acid Dry–Wet Cycle

The study of rock damage is generally described by the variation of macro-mechanical parameters and the evolution of micromorphology. However, the chemical damage

Fig. 14 $\lg[M(x)/M_T]-\lg x$ curve at different pH values

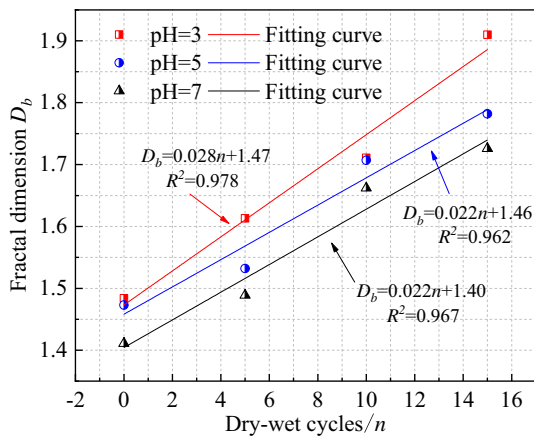
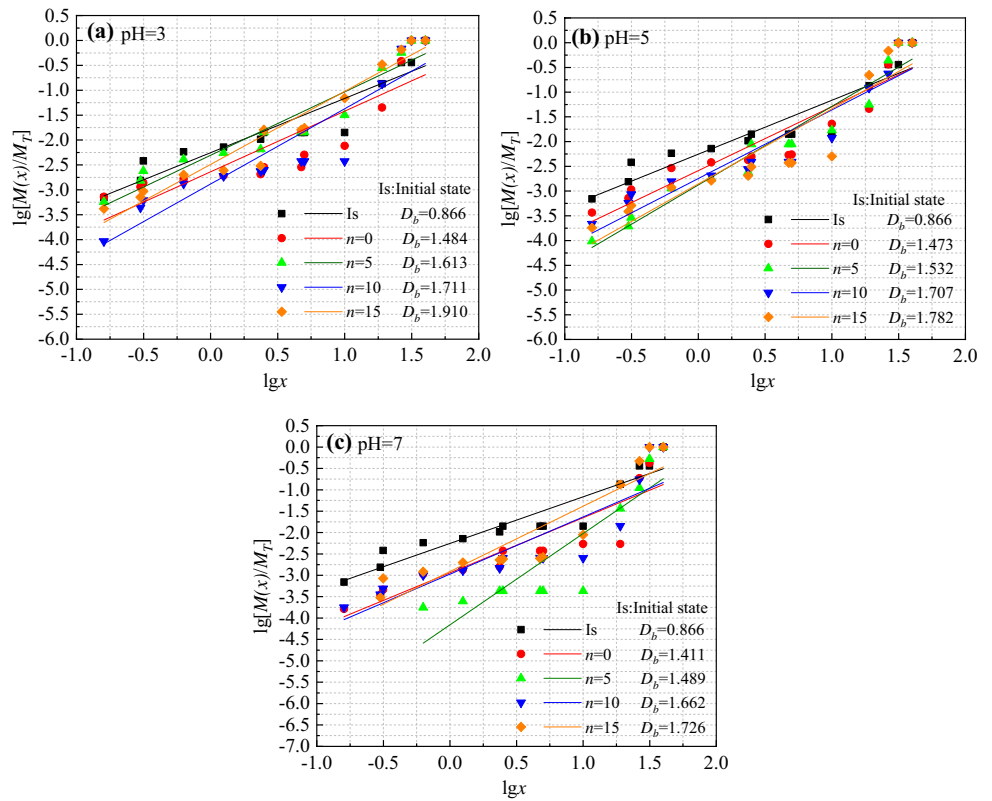


Fig. 15 The relation curve between n and D_b

is not only limited to the micromorphology and structure but also needs to study the relationship between chemical components and chemical damage. In this way, comprehensive information about the micromorphology, structure, and composition of rock surface can be obtained (Chen et al. 2015; Uvarov et al. 2011). The research idea of this section is shown in Fig. 16: the SEM and XRD technology were used, respectively, to study the structural and component changes of sandstone surface before and after acid dry–wet cycle. Then its physical and chemical damage laws were

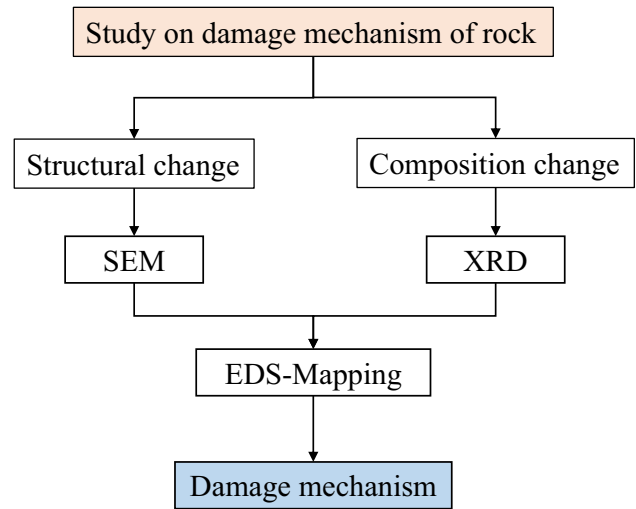


Fig. 16 Research ideas of damage mechanism

summarized, and the EDS Mapping technology was used to locate the change location and composition to further verify the damage mechanism.

With the improvement of spatial resolution of the electron microscope and energy resolution and signal intensity of energy dispersive X-ray spectrometer, surface distribution analysis of elements at nanometer level has been applied more and more in the field of material research (Lu et al. 2014a, b; Titus et al. 2015). The composition and

Fig. 17 Micro-test equipment: **a** SmartLab 18 KW XRD, **b** FEI Versa3D SEM, and **c** EDAX OCTANE PLUS EDS Mapping

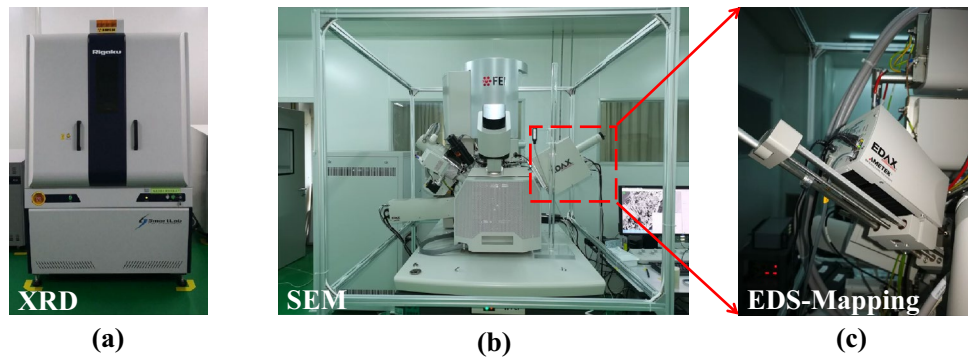
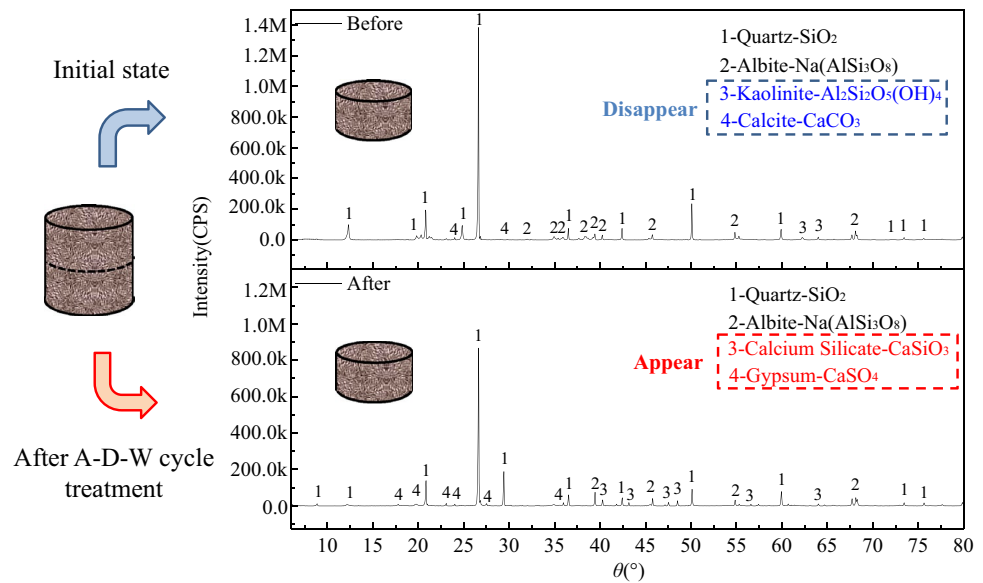


Fig. 18 Changes of substances before and after acid dry–wet cycle treatment



morphology distribution of sandstone surface before and after reaction can be analyzed intuitively, quickly, and accurately by using X-ray diffraction technology, electron microscope, and equipped EDS Mapping (see Fig. 17) (Arizio et al. 2013; Chang et al. 2014; Newbury and Ritchie 2013).

4.1 Change of Substance Before and After the Reaction

To avoid the discreteness of the rock test, a whole sandstone specimen was selected and divided into two blocks, one without any treatment, the other was treated with acid dry–wet cycle following the test group, and the difference of XRD diffraction patterns before and after the reaction was compared (see Fig. 18).

The X-ray diffraction patterns of the specimen before and after the test show that the main materials on the surface of the specimen are still quartz (SiO₂) and feldspar (Albite Na(AlSi₃O₈)). The content of the original kaolinite (Al₂Si₂O₅(OH)₄) and calcite (CaCO₃) in the specimen area is

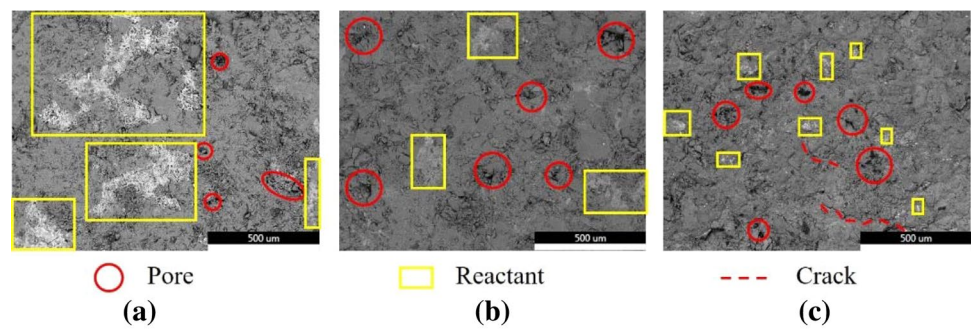
too small to be marked. In addition, new products of calcium silicate (CaSiO₃) and gypsum (CaSO₄) appear.

4.2 Material Distribution and Evolution in the Reaction Process

The whole sandstone specimen was divided into 3 parts and treated by acid dry–wet cycle, respectively. The specimens before reaction (initial state), during the reaction (pH = 3, $n = 5$), and after reaction (pH = 3, $n = 15$) were selected. The surface microstructure and element distribution of the samples were analyzed by electron microscope and EDS Mapping. The surface microstructure was photographed (see Fig. 19).

There were a small number of primary pores and scattered large areas of high brightness material on the original sandstone surface (see Fig. 19a). After 5 times acid dry–wet cycles, the pores on the surface (see Fig. 19b) increased obviously, and the area of high brightness material decreased rapidly. After 15 cycles, the surface of the sandstone (see Fig. 19c) was destroyed obviously. The pores

Fig. 19 Surface microstructure of sandstone in different states: **a** initial state, **b** pH=3 $n=5$ and, **c** pH=3 $n=15$



were developed in a large number and connected (Liu et al. 2018b). Meanwhile, cracks were produced. The high brightness materials gradually disappeared and only existed in a small area. It shows that the acid solution can react with high brightness materials, and can promote the generation and development of cracks in the rock itself. To understand the chemical damage process, we further analyze the material composition on the surface of sandstone, and the material distribution on the surface of sandstone is shown in Fig. 20.

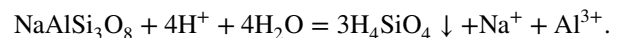
The chemical elements contained in sandstone are mainly Si, O, Al, Fe, S, K, Na, Mg, C, etc. The surface of the specimen was scanned point by point to determine the element with the highest content at each point and marked with different colors (see the upper left corner of Fig. 20). Combining with the diffraction results in Fig. 18, Fe, Ca, Na, S, Al, and Si were selected as characteristic elements. The distribution and abundance of elements in this area were obtained by EDS Mapping analysis. The higher the brightness, the higher the abundance (see Fig. 20, middle and right). The results show that the island area mainly contains Fe, Ca, Na, S, etc., which proves that the area is mainly composed of metal ore (FeO) and calcite (CaCO₃) which are easy to react with the acid solution. The other elements are Si and Al, mainly in the form of quartz (SiO₂), albite (Na(AlSi₃O₈)), and kaolinite (Al₂Si₂O₅(OH)₄). In addition, with the reaction going on, it can be observed that the area of the island area decreases gradually, the distribution area of Fe, Ca, and other elements in the island area decreases gradually, and the area occupied by the Si element increases gradually. The island area was selected as Region 1, and other regions as Region 2. Diffraction analysis was carried out (see Fig. 20, bottom). The signal intensity of Ca, Fe, and Mg in Region 1 decreased continuously, indicating that the element content was decreasing. In Region 2, the content of Al decreases, while the content of Si increases gradually. The above phenomena show that the metal ore and calcite on the surface of sandstone are first lost by acid dry–wet cycles, forming pores and exposing quartz matrix. Under the action of the dry–wet cycle, quartz

particles crack under the combined action of repeated expansion and contraction and acid erosion, which is consistent with the SEM change process described in Fig. 19. It should be noted that the content of the S element fluctuates in a small range in this process. According to the XRD diffraction results in Fig. 18 and the distribution area of the S element in Fig. 20, in addition to the S element in the specimen itself, free Ca²⁺ combines with SO₄²⁻ ion in the acid solution to form gypsum, which is distributed in the island area. However, the substance does not exist stably and will gradually disappear during the continuous dry–wet cycle.

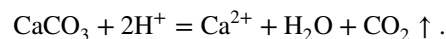
The related reactions were as follows (Feng et al. 2010; Wu et al. 2008):

1. The main reactions in the island region were as follows:

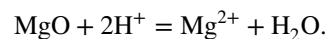
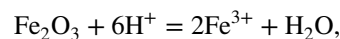
Albite (NaAlSi₃O₈) reacts with H⁺ in an acidic environment to form Na⁺, Al³⁺, and precipitated orthosilicic acid (H₄SiO₄). The specific reaction equation was as follows:



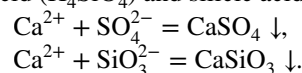
The reaction equation of calcite (CaCO₃) with acid was as follows:



The reaction of metal ores with the acid solution was as follows:



Free Ca²⁺ ions combine with SO₄²⁻ ions to form gypsum (CaSO₄). Free Ca²⁺ ions combine with SiO₃²⁻ ions to form calcium silicate (CaSiO₃). Calcium silicate adheres to the surface of specimens with orthosilicic acid (H₄SiO₄) and silicic acid (H₂SiO₃).



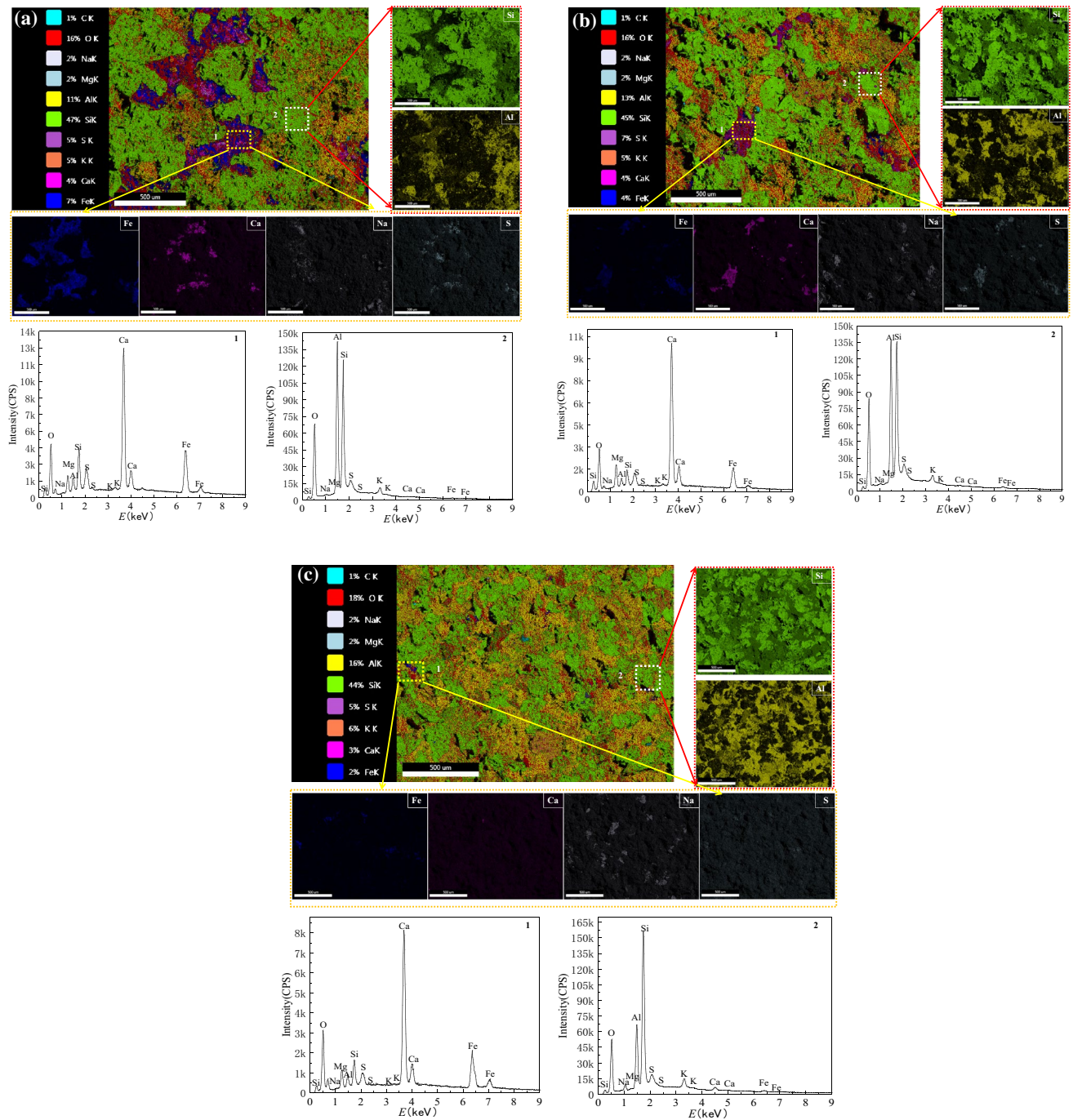
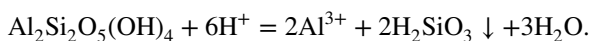


Fig. 20 SEM morphology, element distribution, and X-ray energy spectrum analysis results of micro-region 1, 2: **a** initial state, **b** pH=3 $n=5$, and **c** pH=3 $n=15$

2. Other regions were as follows:

Quartz hardly reacts with acid. The reaction equation of kaolinite ($\text{Al}_2\text{Si}_2\text{O}_5(\text{OH})_4$) with acid was as follows:



4.3 Damage Mechanism of Sandstone Under Dry-Wet Cycle in the Sulfuric Acid Environment

According to the above analysis of XRD, SEM, and EDS Mapping results, it is concluded that the damage mechanism of the dry-wet cycle in the sulfuric acid environment mainly includes two aspects: chemical damage and physical damage (Gan et al.

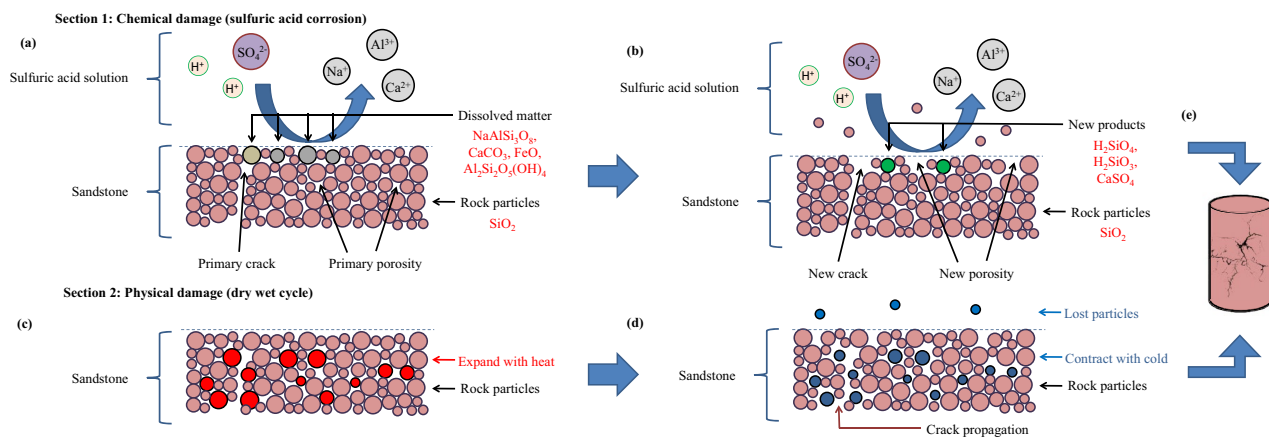


Fig. 21 Sandstone damage mechanism: **a** sulfuric acid dissolution, **b** porosity increase, **c** rock particles expand with heat, **d** rock particles contract with cold, and **e** crack propagation and failure

2021). Compared with the traditional dry–wet cycle medium is water, sulfuric acid in this test has strong corrosivity, which will dissolve oxides and salts on the surface of sandstone at the initial stage of immersion, resulting in the formation of pores (see Fig. 21a). Gypsum and orthosilicic acid are produced during the reaction of sulfuric acid and sandstone, which will adhere to the surface of the specimen and slow down the rate of pore formation to a certain extent (see Fig. 21b); however, with the dry–wet cycle, the substance will gradually dissolve. In addition, the high temperature in the drying stage will cause the rock particles to expand (see Fig. 21c), while the soaking stage will cause the particles to shrink and lose (see Fig. 21d) (Zhao et al. 2018). The alternation of the above two will reduce the connection between rock particles and lead to the formation of cracks (Song et al. 2018). The formation of cracks will further promote chemical corrosion, and eventually lead to the increase of rock pores, crack propagation, and damage (see Fig. 21e).

5 Conclusion

In this paper, the dynamic mechanical properties of sandstone specimens in acid solution with different pH values were studied by the one-dimensional impact dynamic test of coal mine sandstone. The microscopic characteristics of sandstone under different conditions were analyzed, and the damage mechanism of sandstone under the acid dry–wet cycle was summarized. The following conclusions are obtained.

1. One-dimensional impact tests were carried out on the specimens treated by acid dry–wet cycles using SHPB apparatus; the results show that with the decrease of pH

and the increase of cycle times, the dynamic peak stress and modulus of elasticity decrease obviously, and the peak strain increases gradually. Degradation of dynamic mechanical parameters of sandstone in acidic solutions is greater than in neutral.

2. Through the analysis of macro fracture morphology and fractal dimension, it can be observed that with the increase of the number of acid dry–wet cycles, the fragmentation degree of the specimen gradually increases, showing the characteristics of a large number of broken pieces and small particle size, and the fractal dimension also increases.
3. A comprehensive method combining XRD, SEM, and EDS Mapping techniques for rock chemical damage analysis is proposed. The qualitative analysis of element distribution on the surface of sandstone shows that sulfuric acid solution reacts with metal minerals and salts in island distribution on the surface in the process of dry–wet cycles to open the pores, further dissolve other substances, and destroy the structure of the specimen, and gypsum and other substances will be produced in the process.
4. The damage mechanism of sandstone in a sulfuric acid environment was studied. Sandstone is destroyed under the interaction of physical and chemical damage. The sulfuric acid solution can corrode and dissolve oxides and salts on the sandstone surface, resulting in increased pores. Meanwhile, the repeated expansion and contraction of sandstone particles resulted in the development of cracks. Both of them promote each other and lead to the failure of rock specimens.

Acknowledgements The authors acknowledge the School of Civil Engineering and Architecture, Anhui University of Science and Technology for their support to perform this research.

Author contributions XH performed the experiments and analyzed the test data; XH wrote the manuscript; JP conceived the experiment and provided guidance and suggestion. JZ provided important guidance in the process of experimental design, micro-image analysis, and paper modification.

Funding None.

Declarations

Conflicts of interest The authors declare no conflicts of interest.

References

- Arizio E, Orsega EF, Sommariva G, Falcone R (2013) Tin amalgam mirrors: investigation by XRF, SEM-EDS, XRD and EPMA-WDS mapping. *Appl Phys A* 111(3):733–745
- Cai X, Zhou Z, Tan L, Zang H, Song Z (2020a) Fracture behavior and damage mechanisms of sandstone subjected to wetting-drying cycles. *Eng Fract Mech* 234:107109
- Cai X, Zhou Z, Zang H et al (2020b) Water saturation effects on dynamic behavior and microstructure damage of sandstone: phenomena and mechanisms. *Eng Geol* 276:105760
- Cai X, Cheng Q, Zhou Z et al (2021) Rock mass watering for rock-burst prevention: some thoughts on the mechanisms deduced from laboratory results. *Bull Eng Geol Environ*. <https://doi.org/10.1007/s10064-021-02467-0>
- Chang H, Cheng C, Huang P, Lin S (2014) Application of scanning electron microscopy and X-ray microanalysis: FE-SEM, ESEM-EDS, and EDS mapping for studying the characteristics of topographical microstructure and elemental mapping of human cardiac calcified deposition. *Anal Bioanal Chem* 406(1):359–366
- Chen L, Iyengar S, Zhou J, Turba K, Stahl J (2015) Characterization of microstructure and mechanical properties of high chromium cast irons using SEM and nanoindentation. *J Mater Eng Perform* 24(1):98–105
- Chen Z, Shao X, Xu X, He X (2018) Optimized digital speckle patterns for digital image correlation by consideration of both accuracy and efficiency. *Appl Optics* 57(4):884–893
- Ciantia MO, Castellanza R, Crosta GB, Hueckel T (2015) Effects of mineral suspension and dissolution on strength and compressibility of soft carbonate rocks. *Eng Geol* 184:1–18
- Critelli T, Marini L, Schott J et al (2014) Dissolution rates of actinolite and chlorite from a whole-rock experimental study of metabasalt dissolution from $2 \leq \text{pH} \leq 12$ at 25 degrees C. *Chem Geol* 390:100–108
- Dehestani A, Hosseini M, Beydokhti AT (2020) Effect of wetting-drying cycles on mode I and mode II fracture toughness of sandstone in natural (pH=7) and acidic (pH=3) environments. *Theor Appl Fract Mech* 107:102512
- Deng H, Xiao Z, Li J, Hu Y, Zhou M (2015) Deteriorating change rule test research of damage sandstone strength under water-rock interaction. *Chin J Rock Mech Eng (chin)* 34(1):2690–2698
- Du B, Bai H (2019) A damage constitutive model of red sandstone under coupling of wet-dry cycles and impact load. *Shock Vib* 2019:7692424
- Du B, Bai H, Wu G (2019) Dynamic compression properties and deterioration of red-sandstone subject to cyclic wet-dry treatment. *Adv Civ Eng* 2019:1487156
- Fang J, Deng H, Qi Y, Xiao Y, Zhang H, Li J (2019) Analysis of changes in the micromorphology of sandstone joint surface under dry-wet cycling. *Adv Mater Sci Eng* 2019:8758203
- Feng X, Ding W, Cui Q (2010) Coupled chemical-stress effect on rock fracturing process. Science Press, Beijing
- Gan ZQ, Pan X, Tang HZ et al (2021) Experimental investigation on mixed mode I-III fracture characteristics of sandstone corroded by periodic acid solution. *Theor Appl Fract Mech* 114:103034
- Guo Q, Su H, Jing H, Zhu W (2020) Effect of wetting-drying cycle on the deformation and seepage behaviors of rock masses around a tunnel. *Geofluids* 2020:4237163
- Han G, Jing H, Liu R, Su H, Wu J, We J (2019a) Experimental investigation on the mechanical behavior of red sandstone under the coupled effects of temperature and acidic etching. *Arab J Geosci* 12:58618
- Han T, Wang X, Li D, Li D, Han N, Xing F (2019b) Damage and degradation mechanism for single intermittent cracked mortar specimens under a combination of chemical solutions and dry-wet cycles. *Constr Build Mater* 213:567–581
- He LP, Yu JY, Hu QJ, Cai QJ, Qu MF, He TJ (2020) Study on crack propagation and shear behavior of weak muddy intercalations submitted to wetting-drying cycles. *B Eng Geol Environ* 79(9):4873–4889
- Hu M, Liu Y, Ren J, Wu R, Zhang Y (2019) Laboratory test on crack development in mudstone under the action of dry-wet cycles. *B Eng Geol Environ* 78(1):543–556
- Huang X, Pang J, Liu G, Chen Y (2020) Experimental study on physico-mechanical properties of deep sandstone by coupling of dry-wet cycles and acidic environment. *Adv Civ Eng* 2020:2760952
- ISRM (1981) Method for determining uniaxial compressive strength and deformability of rock materials rock characterization testing and monitoring. *Int J Rock Mech Min Sci* 18(6):113–116
- Jiang Q, Deng H, Li J et al (2019) The degradation effect and mechanism by water-rock interaction in the layered sandstone in the three gorges reservoir area. *Arab J Geosci* 12:72223
- Li S, Li C, Yao W et al (2019) Impact of wetting-drying cycles on dynamic tensile strength of rock. *Therm Sci* 233:815–820
- Li Y, Zhang S, Zhang X (2018) Classification and Fractal Characteristics of Coal Rock Fragments Under Uniaxial Cyclic Loading Conditions. *Arab J Geosci* 11:2019
- Liang H, Fu Y (2020) Fracture properties of sandstone degradation under the action of drying-wetting cycles in acid and alkaline environments. *Arab J Geosci* 13:2
- Liang H, Yuan W, Fu Y et al (2021) Degradation law of mixed-mode (I/II) fracture toughness of sandstone under drying-wetting cycles in acid and alkaline environments. *Arab J Geosci* 14(14):1312
- Liu J, Wang Z, Hu S (1998) The SHPB experiment technology for low wave impedance porous materials. *J Exp Mech (chin)* 13(2):3–5
- Liu X, Wang Z, Fu Y, Yuan W, Miao L (2016) Macro/microtesting and damage and degradation of sandstones under dry-wet cycles. *Adv Mater Sci Eng* 2016:7013032
- Liu X, Yuan W, Fu Y, Wang Z, Miao L, Bw X (2018a) Porosity Evolution of Sandstone Dissolution Under Wetting and Drying Cycles. *Chin J Geotech Eng (chin)* 40(3):527–532
- Liu X, Jin M, Li D, Zhang L (2018b) Strength deterioration of a shaly sandstone under dry-wet cycles: a case study from the three gorges reservoir in China. *B Eng Geol Environ* 77(4):1607–1621
- Liu W, Song X, Huang F, Hu L (2019) Experimental Study on the disintegration of granite residual soil under the combined influence of wetting-drying cycles and acid rain. *Geomat Nat Haz Risk* 10(1):1912–1927
- Liu G, Huang X, Pang J (2020) The uniaxial creep characteristics of red sandstone under dry-wet cycles. *Adv Civ Eng* 2020:8841773
- Lu P, Romero E, Lee S, Macmanus-Driscoll JL, Jia Q (2014a) Chemical quantification of atomic-scale EDS maps under thin specimen conditions. *Microsc Microanal* 20(6):1782–1790
- Lu P, Zhou L, Kramer MJ, Smith DJ (2014b) Atomic-scale chemical imaging and quantification of metallic alloy structures by energy-dispersive X-Ray spectroscopy. *Sci Rep-UK* 4:3945

- Ma J, Niu X, Xiong C et al (2020) Experimental investigation of the physical properties and microstructure of slate under wetting and drying cycles using micro-CT and ultrasonic wave velocity tests. *Sens (basel, Switzerl)* 20:17
- Meng B, Jing H, Zhu W, Su H (2019) Influences of saturation and wetting-drying cycle on mechanical performances of argillaceous limestones from liupanshan tunnel, China. *Adv Mater Sci Eng* 2019:9236172
- Newbury DE, Ritchie NWM (2013) Elemental mapping of microstructures by scanning electron microscopy-energy dispersive X-ray spectrometry (SEM-EDS): extraordinary advances with the silicon drift detector (SDD). *J Anal Atom Spectrom* 28(7):973–988
- Shan S, Li Z (2003) Fractal theory, characteristics and its application on rock fragmentation. *J Hebei Inst Technol Chin* 25(2):11–17
- Song L, Hu S (2005) Two-wave and three-wave method in SHPB data processing. *Explos Shock Waves Chin* 25(4):368–373
- Song Z, Ji H, Jiang H, Liu Z, Wang H, Liu Y (2018) Influence of wetting-drying cycles on acoustic emission characteristics and microstructure deterioration of weak cementation stratum. *J China Coal Soc Chin* 43(1):96–103
- Sun Q, Zhang Y (2019) Combined effects of salt, cyclic wetting and drying cycles on the physical and mechanical properties of sandstone. *Eng Geol* 248:70–79
- Titus MS, Mottura A, Viswanathan GB, Suzuki A, Mills MJ, Pollock TM (2015) High resolution energy dispersive spectroscopy mapping of planar defects in L1(2)-containing co-base superalloys. *Acta Mater* 89:423–437
- Uvarov V, Popov I, Shapur N et al (2011) X-ray diffraction and SEM study of kidney stones in Israel: quantitative analysis, crystallite size determination, and statistical characterization. *Environ Geochem Hlth* 33(6):613–622
- Wang Z, Zhu Z, Sun X, Wang X (2017) Deterioration of fracture toughness of concrete under acid rain environment. *Eng Fail Anal* 77:76–84
- Wu X, Zhu B, Luo J (2008) Weathering process of black rock stratum and its thermodynamic analysis. Science Press, Beijing
- Xu J, Liu S (2012) Research on fractal characteristics of marble fragments subjected to impact loading. *Rock Soil Mech Chin* 33(11):3225–3229
- Yuan P, Ma Q, Zhang H (2014) SHPB tests for light weight foam concrete. *J Vibr Shok Chin* 17:116–119
- Yuan W, Liu X, Fu Y (2019a) Chemical thermodynamics and chemical kinetics analysis of sandstone dissolution under the action of dry-wet cycles in acid and alkaline environments. *B Eng Geol Environ* 78(2):793–801
- Yuan P, Wei N, Ma Q, Chang J (2019b) Coupled effect of water temperature and cyclic wetting and drying on dynamic mechanical characteristics of sandstone. *Adv Civ Eng* 2019:8167651
- Zhang R, Ma D, Su Q, Huang K (2020) Effects of temperature and water on mechanical properties, energy dissipation, and microstructure of argillaceous sandstone under static and dynamic loads. *Shock Vib* 2020:8827705
- Zhao Y, Ren S, Jiang D, Liu R, Wu J, Jiang X (2018) Influence of wetting-drying cycles on the pore structure and mechanical properties of mudstone from simian mountain. *Constr Build Mater* 191:923–931
- Zhou Z, Cai X, Chen L, Cao W, Zhao Y, Xiong C (2017) Influence of cyclic wetting and drying on physical and dynamic compressive properties of sandstone. *Eng Geol* 220:1–12
- Zhou Z, Cai X, Ma D, Chen L, Wang S, Tan L (2018) Dynamic tensile properties of sandstone subjected to wetting and drying cycles. *Constr Build Mater* 182:215–232
- Zhou Z, Cai X, Li X et al (2020) Dynamic response and energy evolution of sandstone under coupled static-dynamic compression: insights from experimental study into deep rock engineering applications. *Rock Mech Rock Eng* 53(3):1305–1331

Publisher's Note Springer Nature remains neutral with regard to jurisdictional claims in published maps and institutional affiliations.